Spatial nematic fluctuation in BaFe_{2}(As_{1−x}P_{x})_{2} revealed by spatially and angle-resolved photoemission spectroscopy

Jonathan Ma, Ming Yi, Gregory Affeldt, Ian Hayes, Chris Jozwiak, Aaron Bostwick, Eli Rotenberg, James Analytis, Robert Birgeneau, and Alessandra Lanzara

Phys. Rev. B **101**, 094515 — Published 26 March 2020

DOI: 10.1103/PhysRevB.101.094515

Spatial nematic fluctuation in $BaFe_2(As_{1-x}P_x)_2$ revealed by spatially resolved angle resolved photoemission spectroscopy

Jonathan Ma,[1,2] Ming Yi,[1,3] Gregory Affeldt,[1,2] Ian Hayes,[1,2]
Chris Jozwiak,[4] Aaron Bostwick,[4] Eli Rotenberg,[4] James
Analytis,[1,2] Robert Birgeneau,[1,2] and Alessandra Lanzara[1,2]

[1]*Department of Physics, University of California, Berkeley, Berkeley, CA 94720, USA*

[2]*Material Sciences Division, Lawrence Berkeley National Laboratory, Berkeley , CA 94720, USA*

[3]*Department of Physics and Astronomy, Rice University, TX 77005, USA*

[4]*Advanced Light Source, Lawrence Berkeley National Laboratory, Berkeley , CA 94720, USA*

(Dated: March 3, 2020)

Abstract

Nematicity, where rotational symmetry is broken while translational symmetry is conserved, is prevalent in high temperature superconductors. In particular, nematic quantum critical point has been universally found near the optimum doping of the superconducting dome of several iron-based superconductor families. In such a regime, evidence for strong nematic fluctuations have been observed. As the precursor to this order, nematic fluctuations emerge before nematicity, providing favorable ground to study how nematic order modifies the electronic structure in the absence of structural distortion. Here we use spatially-resolved angle-resolved photoemission spectroscopy (ARPES) to investigate the correlation between the onset of nematic fluctuations and electronic structure in an optimally-doped $BaFe_2(As_{1-x}P_x)_2$ ($x \sim 0.3$) superconductor. We reveal a strong spatially varying anisotropy of the Fermi surface on a length scale of tens of microns with strong correlation between the changes in the hole and electron Fermi pockets, consistent with the variations expected in the presence of fluctuating nematic order. These results provide direct evidence for spatial nematic fluctuations in the optimal doping regime of iron-based superconductors.

In iron-based superconductors C_4 symmetry is broken in a number of forms, leading to a variety of phases. First, at the structural transition temperature, the lattice is observed to transition from a tetragonal to an orthorhombic phase with reduced rotational symmetry[1],[2],[3]. Second, neutron scattering experiments revealed a stripe anti-ferromagnetic order, where magnetic moments align ferromagnetically along one direction and antiferromagnetically along the orthogonal direction. Magnetic order is reported to occur at[4] or below the structural transition temperature[52]. Last but not the least, electronic nematicity was revealed by an anomalously large in-plane resistivity anisotropy[3], orbital anisotropy via angle resolved photoemission[6] and scanning tunneling microscopy[7]. Nematic fluctuations appear to persist beyond the AFM regime[8] in a large range of doping—from phosphorous[910] to electron-doped[63]and hole-doped[11] iron arsenide superconductors. Such fluctuations are manifested in the form of C_4 symmetry breaking[1213]as reported in magnetometry experiment[9] and optical experiments[1014]. In $Sr_{1-x}Na_xFe_2$ As_2, local structural orthorhombicity, a manifestation of local C_4 symmetry breaking, is observed not only above the structural transition temperature, but also in the reentrant tetragonal phase, suggesting that strong nematic fluctuations, manifested in the form of local orthorhombicity, persists even when long range orthorhombicity is suppressed[15]. The proximity between nematic phase and superconductivity also draws questions about the relationship between the two. Intriguingly, large nematic susceptibility, an indicator of strong nematic fluctuation, is observed across families of iron-based superconductors[1617] near optimal doping. The prevalence of nematic fluctuations[9103] and the associated susceptibility near optimal doping suggests that nematic fluctuations may play an important role in mediating superconductivity[16].

It is therefore fundamental to study the evolution of the electronic structure in the presence of nematic fluctuations. Evidence of electronic nematicity corresponding to the onset of resistivity anisotropy[211] has been reported. While giving valuable insights to the problem, these experiments were performed in the presence of uniaxial strain that detwins the structural twin domains occurring in the nematic phase. However, uniaxial strain itself breaks rotational symmetry and extends the orthorhombic phase into the nematic fluctuation regime[11], blurring the phase boundaries thus introducing ambiguity. On that note, one is uncertain whether the observed symmetry breaking is spontaneous or induced. Spatially resolved measurements on the other hand have the advantage of resolving the local properties without requiring any applied strain[10]. Although valuable, so far most of the experiments

have not directly interrogated the local electronic structure. With evidence of prominent spatial variation in the nematic fluctuation regime[10–15] in this family of iron-based superconductors, a technique to probe the spatially varying electronic structure of this system is needed.

In this paper, we use micro-ARPES to study the local electronic structure of the iron pnictide superconductor, $BaFe_2(As_{1-x}P_x)_2$, with a focus in the optimal regime where long range orthorhombicity is suppressed and optimal superconductivity appears[9–10]. We reveal a strong spatial anisotropy of the electronic structure consistent with the variations expected in the presence of nematicity[18]. Specifically we observe that the electron and hole pockets are locally correlated and the local horizontal elongation of one corresponds to the enlargement of the other. The length scale of the observed variations (micron scale) indicates strong nematic susceptibility, which is consistent with the quantum critical behavior previously observed in $BaFe_2(As_{1-x}P_x)_2$[17–19].

Spatially resolved angle resolved photoemission spectroscopy experiments were performed on an optimally doped $BaFe_2(As_{1-x}P_x)_2$ sample. Single crystals were grown by a self-flux method described in[20].

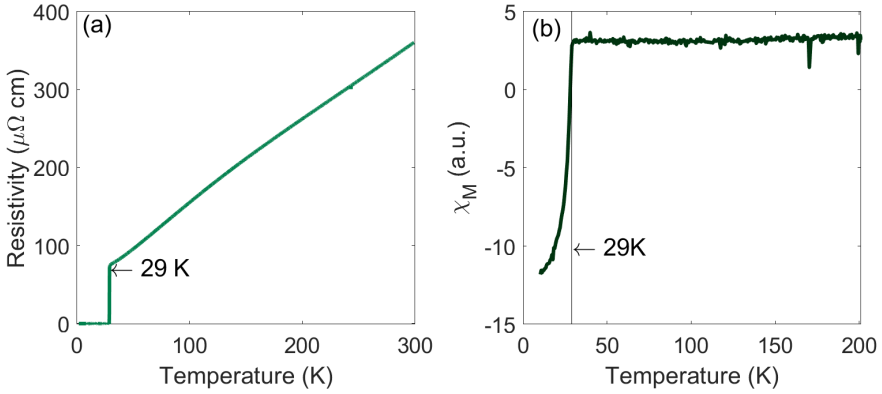

FIG. 1. Resistivity (a) and magnetic susceptibility(b) of the sample measured as a function of temperature

The doping of the sample is confirmed with resistivity and magnetic susceptibility, which were measured as functions of temperature and is consistent with previous reports[21–17]. Susceptibility measurements were made on cooling with a 1 Tesla field in the a-b plane. A DC SQUID magnetometer manufactured by Cryogenic Limited was used. The step at 29 Kelvin in the resistivity curve and the magnetic susceptibility indicates the onset of superconduc-

tivity. The resistivity above 29 Kelvin is a linear function of temperature with no additional feature. Antiferromagnetism (AFM) transition is known to manifest as discontinuities in the resistance-temperature or its first derivative[21]. We observed no such features. Similarly we don't observe AFM features[21] in the magnetic susceptibility curve. Neutron measurements further show that at the doping of x=0.3 and experimental temperature of 20K, AFM does not exist[22].

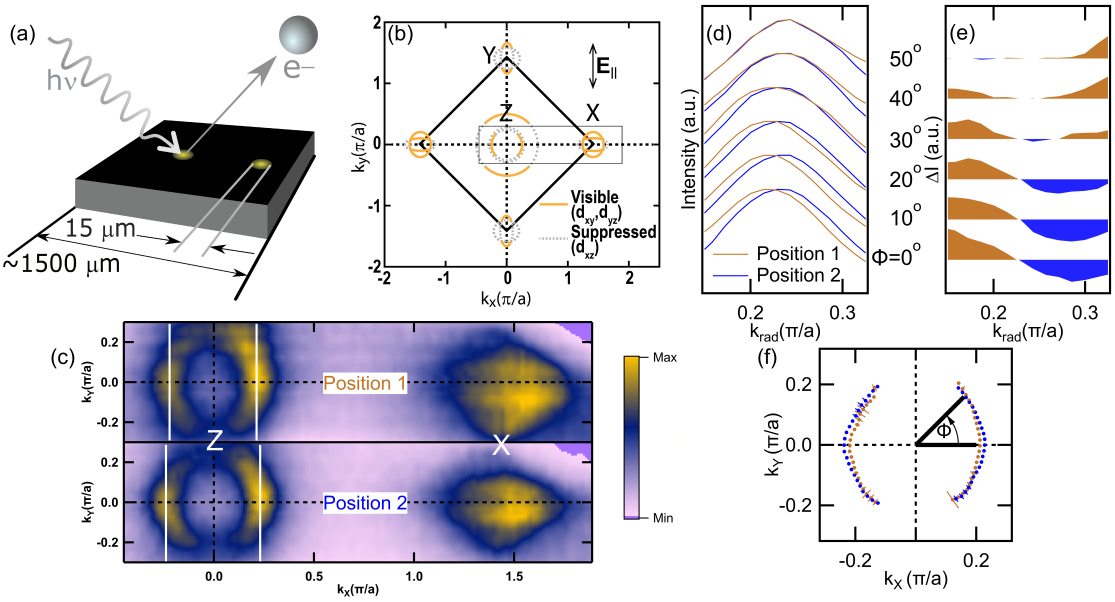

FIG. 2. (a)illustrates spatially resolved ARPES experiment.(b) is a schematic of the Brillouin Zone. (c) juxtaposes two Fermi surfaces taken at two spatial positions with 100 eV photons. (d) Radial MDCs taken from the two positions and (e) the differences between two positions. (f) The extracted Fermi surface of the hole pockets at the two positions in (c).

ARPES data were taken at Beam line 7.0.2 at the Advanced Light Source (ALS). Photon energies 100eV and 120eV, corresponding to $k_z = \pi$ and $k_z = 0$ were used. Unless otherwise specified, all measurements were made at 20K with an energy resolution of 35 meV and momentum resolution better than 0.005 $Å^{-1}$ (0.006 π/a). A custom Scienta R4000 hemispherical electron analyzer with deflector mode was used. Therefore, no sample rotation was needed for Fermi surface mapping, ensuring that the beam stayed on the same sample position. The beam spot size, which is also the spatial resolution, was kept at 15 microns, similar to the reported domain size of iron-pnictides in the orthorhombic phase[23]. The light polarization and photon energy used in this work is mostly sensitive to distinguishing the

d_{yz} and d_{xz} characters of the electronic structure, which is directly involved in the symmetry breaking associated with electronic nematicity in these materials[6241825].

Figure 2a-b show the schematic of the experiment and the hole pocket at Z and electron pocket at X over the first Brillouin zone (black diamond). The schematic Fermi surface is shown for reference in panel b. As previously studied[626], the well defined orbital character of the different Fermi surface sheets allows for selectively enhancing the contributions from different d_{yz}, d_{xy} or d_{xz} components with appropriate light polarization and photon energy. Figure 2c shows the experimental Fermi surface measured at two different spatial positions on the sample with 100eV photons (corresponding to $k_z = \pi$), in agreement with previous results[26]. A quick comparison between the two reveals an overall elongation of the hole pocket size and a narrowing of the electron pocket, moving from position 1 to position 2.

To extract the Fermi surfaces shown in figure 2 c, radial momentum distribution curve (MDC) peak positions are obtained by Lorentzian fitting with a cubic background. The shift in MDCs peak positions becomes more pronounced as the Fermi surface angle Φ decreases (panel d,e), suggesting a different degree of elongation of the hole pocket. This can be seen in greater details by the direct comparison of the MDCs peak positions along the entire Fermi surface, shown in panel f. Such comparison reveals the overall elongation of the hole pocket: the hole pocket radius at $\Phi = 0$ varies by approximately 0.03 π/a from one position to another which is about 10% of the radius, with the largest deviations along the Z-X direction (angles $\leq$ 30 degrees). Such evolution is also supported by the difference spectra in panel e and summarized in panel f, where the fitted Fermi maps for the two positions are shown. To estimate the uncertainty in Fermi surface measurements, the fitting is repeated with a linear background. The difference between the peak positions produced by using the two background functions (linear and cubic), were taken as the errors bars. Since such differences are significantly larger than the errors reported by the fitting routine, they serve as a conservative estimate of our sensitivity to peak positions.

Similar observations are also made using 120eV photons (corresponding $k_z = 0$). The Fermi surface second derivative spectra shown in figure 3a clearly shows the difference between the two positions.

Figure 3b shows the variation of the hole pocket's diameter along the Γ-X and Γ-Y direction for a collection of beam spots measured using 120 eV photons. The correlation between the two are shown in figure 3c. Each data point corresponds to the pocket size

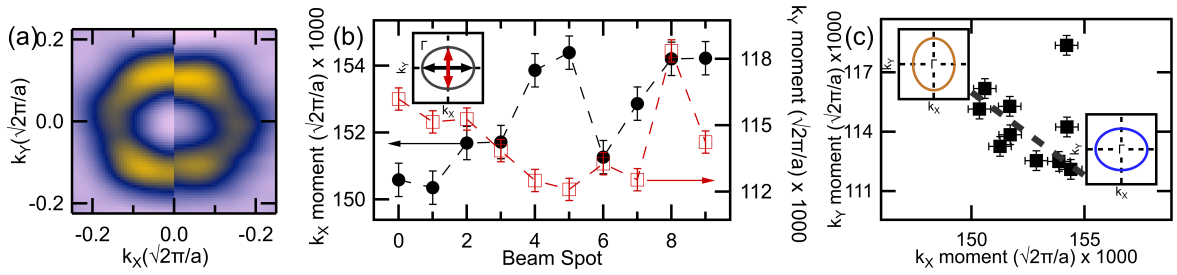

FIG. 3. (a) The momentum second derivatives of the hole pockets measured in two positions with 120 eV photons.(b) Moments of hole pockets taken with 120 eV light as a function of position. Beam spots are equally spaced along a straight line with 33 micron spacing. (c) The relation between the horizontal and vertical moments.

at a beam spot. The location of the Fermi momentum along the two directions is inferred from the second moments, which are calculated by $\sigma_\alpha = \sqrt{[\sum I(k)(k_\alpha - k_0)^2] / [\sum I(k)]}$ ($\alpha = x, y; k_0$: center of mass) along two directions, k_x and k_y. Spectral moment analysis has proven to be informative in superconducting systems[27]. Moment is adopted because it does not make any assumption about the functional form of the MDCs taken from the hole pocket. Also, in comparison to more advanced techniques, such as curve fitting, moment requires fewer manual or discretionary parameters, thus providing more objective results. Moreover, second moments are more sensitive to intensities farther away from the center of mass than first moments. The data show a clear anti-correlation between the moments along k_x and k_y — as the hole pocket widens along k_x, it shrinks along the k_y and vice versa. The k_x moment varies by 3% while the k_y moment varies by 5%.

The moments are evenly distributed across the ranges of variation and our observations indicate that a bimodal distribution, in which data points cluster into two groups, is unlikely. This is also supported by the linear correlation between the two moments shown in panel c, revealing an elliptical type of elongation of the hole pocket as a function of spatial position. This indicates that the continuous variation that we observe is unlikely to be the result of domains with well-defined nematic strength, more in-line with spatially varying nematic fluctuations.

Figure 4 shows the evolution of the electron pocket as a function of position. The electron pocket is measured simultaneously at the same positions as the hole pockets shown in figure 3. A similar procedure to the one used for the hole pockets, is adopted to extract the

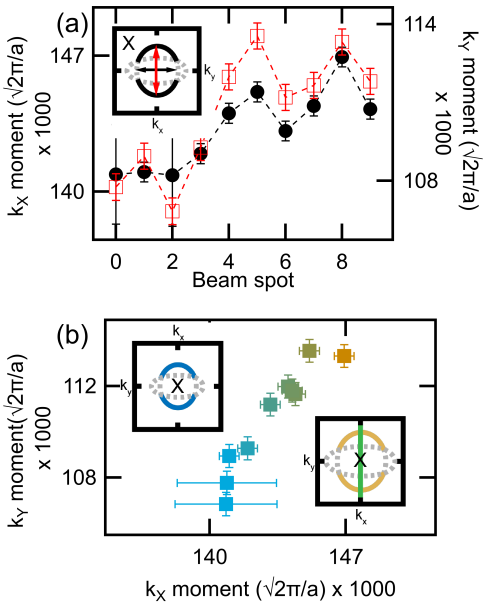

FIG. 4. (a) Electron pocket moments.(b) Relation between horizontal and vertical moments of the electron pockets.

moments of the electron pockets. In contrast to the former, we find that the moments along the Γ-X (k_x) and Γ-Y (k_y) directions for the electron pocket covary—a larger moment along k_y direction corresponds to a larger moment along k_x direction (as schematically illustrated in the inset of figure 4(b)). The variation in both direction is around 5%, comparable to the variation observed for the hole pocket.

To understand our findings in a broader context, figure 5 discusses the correlation between the hole and the electron pockets. Panel (a) shows the elongation of the hole pocket versus the vertical size of the electron pocket. More specifically, the difference between the horizontal ($\sigma_{h,x}$) and the vertical($\sigma_{h,y}$) moments are taken and divided by their sum $\left(\frac{\sigma_{h,x}-\sigma_{h,y}}{\sigma_{h,x}+\sigma_{h,y}}\right)$as a measure of horizontal elongation of the hole pocket. Horizontal elongation is plotted against the vertical (k_y) moment of the electron pocket. As one can see, more horizontally elongated the hole pocket is, the larger the vertical dimension of the electron pocket.

Figures 5(b,c) schematically summarize the findings of our work, revealing a correlation between the elongation of the electron and hole pockets. Specifically, a horizontal elongated hole pocket corresponds to a larger electron pocket (panel b), while a vertical elongated hole pocket corresponds to a smaller electron pocket (panel c).

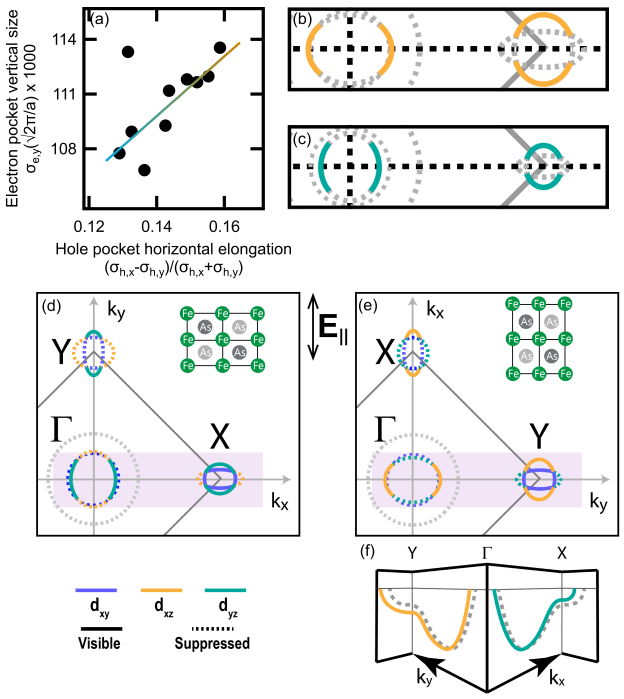

FIG. 5. (a) Elongation of the hole pocket versus the vertical size of the electron pocket. Solid line indicates least absolute error fit. (b,c) Schematic illustrations of the two measured situations showing the correlation between the electron and hole pockets.(e,f) are the schematic Fermi surfaces at orthogonal nematic domains with purple shading highlighting the region measured. (f) illustrates orbital dependent shift in nematic phase.

The presence of such correlation is a manifestation of electronic nematicity[13]. In the bulk nematic phase, depending on the local domain captured by the beam spot, the s polarized light used in this work is mainly measuring the contribution of the d_{yz} or d_{xz} orbitals, which are directly involved in nematic electronic anisotropy[28]. As the system transitions into the bulk nematic phase, the Fe-Fe bond along orthogonal directions become inequivalent[45].

Along the k_x axis, the d_{yz} orbital shifts up near the X point[18] and shifts down near the Γ point as observed in FeSe[2930] and parent compound $BaFe_2As_2$[31] (figure 5f). As a result, the hole pocket will shrink along k_x and the electron pocket near the X point will shrink along k_y as well. As illustrated in figure 5d, the portion of the electron pocket away from the k_x axis has a d_{yz} character which is selected by s-polarized light. Therefore, a widened electron pocket along k_y direction is expected as the entire pocket expands. In an orthogonal domains, as in figure 5e, k_x and k_y axes are rotated by 90 degrees while d_{xz} and d_{yz} orbitals

switch places. As a result, features around the k_y axis are measured while d_{xz} orbitals are selected by s-polarized light with the given experimental geometry. The d_{xz} bands shift in opposite directions as the d_{yz} bands – they shift up near Γ and down near Y (figure 5f). The resemblance between the two observed extrema (figure 5b,c) and anisotropy originated in nematicity (figure 5d,e) suggests that the observed variations are related to nematicity. The rather continuous spread in various correlations points to a fluctuation nature of the observations.

We note that spatial variation in the elongation of the hole pocket suggests that C_4 symmetry is locally broken in a spatially varying manner. Previous works predicted changes in the hole pocket geometry occurs when C_4 symmetry is broken[3233]. High resolution ARPES work indicated that the hole pocket elongates in the presence of nematicity[6342825]. Our observations on the correlation between hole pocket elongation and electron pocket vertical size is similar to the reported sign changing nematicity-induced modification on the electronic structure[18], proposing a link between the observed spatial variation and nematicitic fluctuations. The fact that all measurements were made outside the bulk nematic regime suggests the fluctuating nature of the observed variation.

Finally we note that our observations are inconsistent with a spatially varying phosphorus doping scenario. At 120eV, as phosphorus content increases, one expects the hole pocket to be less horizontally elongated and the electron pocket to enlarge[26]. In contrast, our data show that the more horizontally elongated the hole pocket is, the larger is the electron pocket size. With this inconsistency between our observations and the phosphorus doping scenario, we find spatially varying phosphorus content an unlikely explanation.

In conclusion, we report presence of real space variation in the electronic structure in the presence of nematic fluctuation. This demonstrates a strong correlation between the two as previously predicted[33328]. In general, these results show that micron scale ARPES can be used as an effective tool in characterizing the way nematic fluctuation appears as spatial variations of electronic structure. Further doping and temperature dependent studies are needed to provide a comprehensive picture of the interplay between nematic fluctuations and superconductivity.

We thank D.-H. Lee and E. Thewalt for useful discussions. This work was funded by the U.S. Department of Energy, Office of Science, Office of Basic Energy Sciences, Materials Sciences and Engineering Division under Contract No. DE-AC02-05-CH11231 (Quantum

materials KC2202).

Appendix A: Moment Measurements

Moments were adopted for a few reasons. First, in contrast to curve fitting, no assumptions about the functional form of the spectra is made. Also, fewer manual parameters are needed, reducing subjectivity. Second, unlike peak finding procedures, no smoothing is required. In data taken with 120 eV light, the MDCs of the hole pocket along the k_x direction often don't show a clear two peak feature while k_x MDCs taken at the electron pocket is a single peak. Therefore it is not possible to measure the MDC peak separations for all positions along the k_x direction for both pockets. To improve statistics, moments are not taken with a single MDC. Instead, there is a finite integration window. For hole pocket moments, the integration width is $0.04\sqrt{2}\frac{\pi}{a}$. For electron pockets, the integration widths are $0.3\sqrt{2}\frac{\pi}{a}$ for vertical moments and $0.25\sqrt{2}\frac{\pi}{a}$ for horizontal moments.

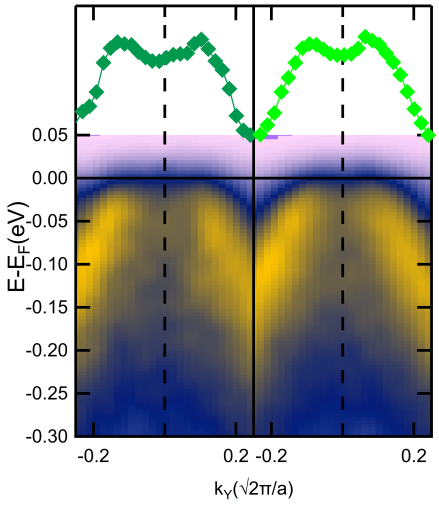

FIG. 6. Electronic dispersion along the Y-Γ-Y direction taken from the two positions measured with 120 eV photons

To illustrate the technique, in FIG 6 two k_y dispersions corresponding to the to positions are shown to be significantly different. The bands on the left are further away from each other than the ones on the right. MDCs are taken at Fermi energy. The peak separation on the left is visually larger than that on the right. Correspondingly, the moment extracted from the left and right panels are $0.1184 \pm 0.0005\sqrt{2}\frac{\pi}{a}$ and $0.1125 \pm 0.0005\sqrt{2}\frac{\pi}{a}$.

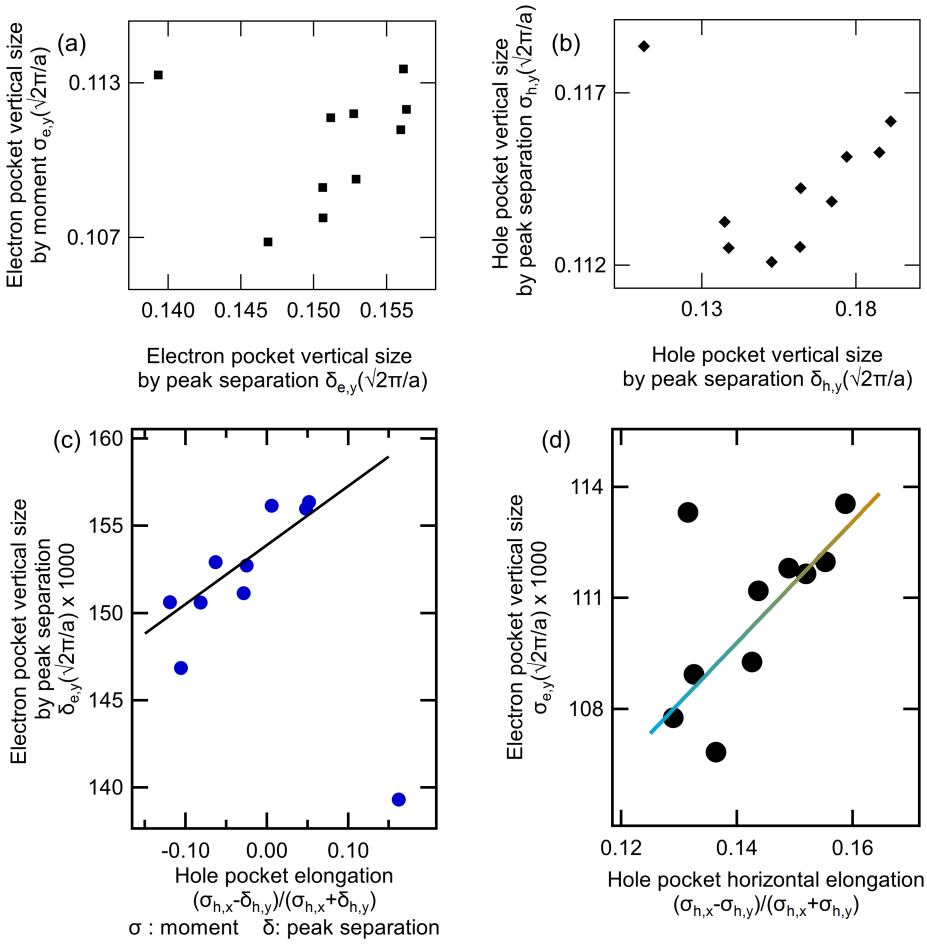

FIG. 7. (a) The relation between vertical MDC peak separation and the vertical moment of the electron pocket. (b) The relation between MDC peak separation and the vertical moment of the hole pocket. (c) vertical MDC peak separation versus $\frac{\sigma_{h,x}-\delta_{h,y}}{\sigma_{h,x}+\delta_{h,y}}$. (d) Vertical moment of the electron pocket versus $\frac{\sigma_{h,x}-\sigma_{h,y}}{\sigma_{h,x}+\sigma_{h,y}}$

The k_y moments are plotted against the k_y MDC peak separation for the electron pocket (Figure 7a) and the hole pocket (Figure 7b). The moment measurements and the respective peak separations are positively correlated. Using the peak separations extracted from k_y MDCs, an alternative way $\left(\frac{\sigma_{h,x}-\delta_{h,y}}{\sigma_{h,x}+\delta_{h,y}}\right)$ is used to measure the degree of hole pocket elongation. As the k_x MDC peak separation cannot be extracted, the k_x moment is retained. Using this alternative, $\left(\frac{\sigma_{h,x}-\delta_{h,y}}{\sigma_{h,x}+\delta_{h,y}}\right)$ positively correlates with the k_y MDC peak separation of the electron pocket, as shown in figure 7c, indicating that more horizontally elongated is the hole pocket, vertically larger is the electron pocket. The alternative is qualitatively consistent with results

using only moment measurements (Figure 7d).

---

[1] Clarina de la Cruz, Q. Huang, J. W. Lynn, Jiying Li, W Ratcliff, J. L. Zarestky, H. A. Mook, G. F. Chen, J. L. Luo, N. L. Wang, and Pengcheng Dai, "Magnetic order close to superconductivity in the iron-based layered $LaO_{1-x}F_xFeAs$ systems." Nature **453**, 899–902 (2008), arXiv:0804.0795.

[2] Jiun Haw Chu, James G. Analytis, Chris Kucharczyk, and Ian R. Fisher, "Determination of the phase diagram of the electron-doped superconductor $Ba(Fe_{1-x}\ Co_x)2\ As_2$," Physical Review B - Condensed Matter and Materials Physics **79**, 1–6 (2009), arXiv:arXiv:1002.4952.

[3] Jiun-Haw Chu, James G. Analytis, Kristiaan De Greve, Peter L. McMahon, Zahirul Islam, Yoshihisa Yamamoto, and Ian R. Fisher, "In-plane resistivity anisotropy in an underdoped iron arsenide superconductor," Science **329**, 824–826 (2010), http://science.sciencemag.org/content/329/5993/824.full.pdf.

[4] S. Avci, O. Chmaissem, D. Y. Chung, S. Rosenkranz, E. A. Goremychkin, J. P. Castellan, I. S. Todorov, J. A. Schlueter, H. Claus, A. Daoud-Aladine, D. D. Khalyavin, M. G. Kanatzidis, and R. Osborn, "Phase diagram of $Ba_{1-x}K_xFe_2As_2$," Physical Review B - Condensed Matter and Materials Physics **85**, 1–12 (2012), arXiv:1205.0489.

[5] N. Ni, M. E. Tillman, J. Q. Yan, A. Kracher, S. T. Hannahs, S. L. Bud'ko, and P. C. Canfield, "Effects of Co substitution on thermodynamic and transport properties and anisotropic H_{c2} in $Ba(Fe_{1-x}Co_x)_2As_2$ single crystals," Physical Review B **78**, 1–9 (2008), arXiv:0811.1767.

[6] Ming Yi, Donghui Lu, Jiun-Haw Chu, James G. Analytis, Adam P. Sorini, Alexander F. Kemper, Brian Moritz, Sung-Kwan Mo, Rob G. Moore, Makoto Hashimoto, Wei-Sheng Lee, Zahid Hussain, Thomas P. Devereaux, Ian R. Fisher, and Zhi-Xun Shen, "Symmetry-breaking orbital anisotropy observed for detwinned $Ba(Fe_{1-x}Co_x)2As_2$ above the spin density wave transition," Proceedings of the National Academy of Sciences **108**, 6878–6883 (2011), https://www.pnas.org/content/108/17/6878.full.pdf.

[7] T.-M. Chuang, M. P. Allan, Jinho Lee, Yang Xie, Ni Ni, S. L. Bud'ko, G. S. Boebinger, P. C. Canfield, and J. C. Davis, "Nematic Electronic Structure in the "Parent" State of the Iron-Based Superconductor $Ca(Fe_{1-x}Co_x)_2As_2$," Science **327**, 181–184 (2010), http://science.sciencemag.org/content/327/5962/181.full.pdf.

[8] Yann Gallais and Indranil Paul, "Charge nematicity and electronic raman scattering in iron-based superconductors," Comptes Rendus Physique **17**, 113 – 139 (2016), iron-based superconductors / Supraconducteurs base de fer.

[9] S. Kasahara, H. J. Shi, K. Hashimoto, S. Tonegawa, Y. Mizukami, T. Shibauchi, K. Sugimoto, T. Fukuda, T. Terashima, Andriy H. Nevidomskyy, and Y. Matsuda, "Electronic nematicity above the structural and superconducting transition in $BaFe_2(As_{1-x}P_x)_2$." Nature **486**, 382–385 (2012), arXiv:1207.1045.

[10] Eric Thewalt, Ian M. Hayes, James P. Hinton, Arielle Little, Shreyas Patankar, Liang Wu, Toni Helm, Camelia V. Stan, Nobumichi Tamura, James G. Analytis, and Joseph Orenstein, "Imaging anomalous nematic order and strain in optimally doped $BaFe_2(As, P)_2$," Phys. Rev. Lett. **121**, 027001 (2018).

[11] E C Blomberg, M a Tanatar, R M Fernandes, I I Mazin, Bing Shen, Hai-Hu Wen, M D Johannes, J Schmalian, and R Prozorov, "Sign-reversal of the in-plane resistivity anisotropy in hole-doped iron pnictides." Nature communications **4**, 1914 (2013), arXiv:1202.4430.

[12] R. M. Fernandes, L. H. Vanbebber, S. Bhattacharya, P. Chandra, V. Keppens, D. Mandrus, M. A. McGuire, B. C. Sales, A. S. Sefat, and J. Schmalian, "Effects of nematic fluctuations on the elastic properties of iron arsenide superconductors," Physical Review Letters **105**, 1–4 (2010), arXiv:0911.3084.

[13] R. M. Fernandes, A. V. Chubukov, J. Knolle, I. Eremin, and J. Schmalian, "Preemptive nematic order, pseudogap, and orbital order in the iron pnictides," Physical Review B - Condensed Matter and Materials Physics **85**, 1–31 (2012), arXiv:1110.1893.

[14] B. Xu, Y. M. Dai, H. Xiao, B. Shen, Z. R. Ye, A. Forget, D. Colson, D. L. Feng, H. H. Wen, X. G. Qiu, and R. P.S.M. Lobo, "Optical observation of spin-density-wave fluctuations in Ba122 iron-based superconductors," Physical Review B **94**, 1–6 (2016), arXiv:1608.05474.

[15] Benjamin A. Frandsen, Keith M. Taddei, Daniel E. Bugaris, Ryan Stadel, Ming Yi, Arani Acharya, Raymond Osborn, Stephan Rosenkranz, Omar Chmaissem, and Robert J. Birgeneau, "Widespread orthorhombic fluctuations in the (Sr,Na)Fe_2 As_2 family of superconductors," Phys. Rev. B **98**, 180505 (2018).

[16] Hsueh-Hui Kuo, Jiun-Haw Chu, Johanna C. Palmstrom, Steven A. Kivelson, and Ian R. Fisher, "Ubiquitous signatures of nematic quantum criticality in optimally doped Fe-based superconductors," Science **352**, 958–962 (2016),

https://science.sciencemag.org/content/352/6288/958.full.pdf.

[17] Ian M. Hayes, Ross D. McDonald, Nicholas P. Breznay, Toni Helm, Philip J. W. Moll, Mark Wartenbe, Arkady Shekhter, and James G. Analytis, "Scaling between magnetic field and temperature in the high-temperature superconductor $BaFe_2(As_{1-x}P_x)_2$," Nature Physics **12**, 4–7 (2016), arXiv:1412.6484.

[18] Ming Yi, Yan Zhang, Zhi-Xun Shen, and Donghui Lu, "Role of the orbital degree of freedom in iron-based superconductors," npj Quantum Materials **2**, 57 (2017), arXiv:1703.08622.

[19] James G Analytis, H H Kuo, Ross D McDonald, Mark Wartenbe, P M C Rourke, N E Hussey, and I R Fisher, "Transport near a quantum critical point in $BaFe_2(As_{1-x}P_x)_2$," Nature Physics **10**, 1–4 (2014).

[20] J. G. Analytis, J. H. Chu, R. D. McDonald, S. C. Riggs, and I. R. Fisher, "Enhanced fermi-surface nesting in superconducting $BaFe_2(As_{1-x}P_x)_2$ revealed by the de Haas-van alphen effect," Physical Review Letters **105**, 1–4 (2010).

[21] S. Kasahara, T. Shibauchi, K. Hashimoto, K. Ikada, S. Tonegawa, R. Okazaki, H. Shishido, H. Ikeda, H. Takeya, K. Hirata, T. Terashima, and Y. Matsuda, "Evolution from non-Fermi- to Fermi-liquid transport via isovalent doping in $BaFe_2(As_{1-x}P_x)_2$ superconductors," Phys. Rev. B **81**, 184519 (2010).

[22] Ding Hu, Xingye Lu, Wenliang Zhang, Huiqian Luo, Shiliang Li, Peipei Wang, Genfu Chen, Fei Han, Shree R. Banjara, A. Sapkota, A. Kreyssig, A. I. Goldman, Z. Yamani, Christof Niedermayer, Markos Skoulatos, Robert Georgii, T. Keller, Pengshuai Wang, Weiqiang Yu, and Pengcheng Dai, "Structural and magnetic phase transitions near optimal superconductivity in $BaFe_2(As_{1-x}P_x)_2$," Phys. Rev. Lett. **114**, 157002 (2015).

[23] M. A. Tanatar, A. Kreyssig, S. Nandi, N. Ni, S. L. Bud'ko, P. C. Canfield, A. I. Goldman, and R. Prozorov, "Direct imaging of the structural domains in the iron pnictides AFe_2As_2 (A = Ca , Sr , Ba)," Physical Review B **79**, 180508 (2009).

[24] M. Yi, Y. Zhang, Z.-K. Liu, X. Ding, J.-H. Chu, a F Kemper, N. Plonka, B. Moritz, M. Hashimoto, S.-K. Mo, Z. Hussain, T P Devereaux, I R Fisher, H H Wen, Z.-X. Shen, and D H Lu, "Dynamic competition between spin-density wave order and superconductivity in underdoped $Ba_{1-x}K_xFe_2As_2$." Nat. Commun. **5**, 3711 (2014).

[25] Y. Zhang, C. He, Z. R. Ye, J. Jiang, F. Chen, M. Xu, Q. Q. Ge, B. P. Xie, J. Wei, M. Aeschlimann, X. Y. Cui, M. Shi, J. P. Hu, and D. L. Feng, "Symmetry breaking via orbital-dependent

reconstruction of electronic structure in detwinned NaFeAs," Physical Review B - Condensed Matter and Materials Physics **85**, 1–12 (2012), arXiv:1111.6430.

[26] Z. R. Ye, Y. Zhang, F. Chen, M. Xu, Q. Q. Ge, J. Jiang, B. P. Xie, and D. L. Feng, "Doping dependence of the electronic structure in phosphorus-doped ferropnictide superconductor $BaFe_2(As_{1-x}P_x)_2$ studied by angle-resolved photoemission spectroscopy," Physical Review B - Condensed Matter and Materials Physics **86**, 1–8 (2012), arXiv:1105.5242.

[27] Makoto Hashimoto, Elizabeth A. Nowadnick, Rui-Hua He, Inna M. Vishik, Brian Moritz, Yu He, Kiyohisa Tanaka, Robert G. Moore, Donghui Lu, Yoshiyuki Yoshida, Motoyuki Ishikado, Takao Sasagawa, Kazuhiro Fujita, Shigeyuki Ishida, Shinichi Uchida, Hiroshi Eisaki, Zahid Hussain, Thomas P. Devereaux, and Zhi-Xun Shen, "Direct spectroscopic evidence for phase competition between the pseudogap and superconductivity in $Bi_2Sr_2CaCu_2O_{8+\delta}$," Nature Materials **14**, 37–42 (2015).

[28] M. Yi, D. H. Lu, R. G. Moore, K. Kihou, C. H. Lee, A. Iyo, H. Eisaki, T. Yoshida, A. Fujimori, and Z. X. Shen, "Electronic reconstruction through the structural and magnetic transitions in detwinned NaFeAs," New Journal of Physics **14** (2012), 10.1088/1367-2630/14/7/073019, arXiv:1111.6134.

[29] Y. Zhang, M. Yi, Z.-K. Liu, W. Li, J. J. Lee, R. G. Moore, M. Hashimoto, M. Nakajima, H. Eisaki, S.-K. Mo, Z. Hussain, T. P. Devereaux, Z.-X. Shen, and D. H. Lu, "Distinctive orbital anisotropy observed in the nematic state of a fese thin film," Phys. Rev. B **94**, 115153 (2016).

[30] M. Yi, H. Pfau, Y. Zhang, Y. He, H. Wu, T. Chen, Z. R. Ye, M. Hashimoto, R. Yu, Q. Si, D.-H. Lee, Pengcheng Dai, Z.-X. Shen, D. H. Lu, and R. J. Birgeneau, "Nematic Energy Scale and the Missing Electron Pocket in FeSe," Phys. Rev. X **9**, 041049 (2019).

[31] H. Pfau, S. D. Chen, M. Yi, M. Hashimoto, C. R. Rotundu, J. C. Palmstrom, T. Chen, P.-C. Dai, J. Straquadine, A. Hristov, R. J. Birgeneau, I. R. Fisher, D. Lu, and Z.-X. Shen, "Momentum dependence of the nematic order parameter in iron-based superconductors," Phys. Rev. Lett. **123**, 066402 (2019).

[32] R. M. Fernandes, a. V. Chubukov, and J. Schmalian, "What drives nematic order in iron-based superconductors?" Nature Physics **10**, 97–104 (2014), arXiv:1312.6085 [cond-mat.str-el].

[33] Yuehua Su, Haijun Liao, and Tao Li, "The form and origin of orbital ordering in the electronic nematic phase of iron-based superconductors," Journal of Physics: Condensed Matter

27, 105702 (2015), arXiv:1402.5209.

[34] M. Yi, D. H. Lu, J. G. Analytis, Jiun-Haw H. Chu, S.-K. K. Mo, R.-H. H. He, M. Hashimoto, R. G. Moore, Igor I. Mazin, D. J. Singh, Z. Hussain, I. R. Fisher, and Z.-X. X. Shen, "Unconventional electronic reconstruction in undoped (Ba,Sr)Fe_2As_2 across the spin density wave transition," Physical Review B **80**, 1–10 (2009), arXiv:arXiv:0909.0831v1.